DESIGN AND ANALYSIS OF A COOLING INSERTION LATTICE FOR OPTICAL STOCHASTIC COOLING*

A. Zholents and M. Zolotorev

Accelerator and Fusion Research Division,
E.O. Lawrence Berkeley National Laboratory, Berkeley, CA 94720

W. Wan
University of Colorado, Boulder, CO 80309

1 INTRODUCTION

In this paper we consider an example of a highly isochronous beam line that can be used in the Optical Stochastic Cooling method [1], [2] to bypass an optical amplifier. As it is stated in [1], there are stringent requirements on the time-of-flight properties of the bypass lattice employed in a cooling scheme. Namely, it is necessary to preserve relative longitudinal positions of particles inside the bunch from the beginning to the end of the bypass with the accuracy of $\lambda/2\pi$, where $\lambda \simeq 0.6\,\mu m$ is a carrying (optical) wavelength. At first glance, $\lambda/2\pi$ is such a small value that reaching this accuracy looks nearly impossible. However, simulations show that a carefully designed bypass can meet all the requirements even with rather conservative tolerance to errors. Currently, we are planing to build a highly isochronous beam line where we can learn how to handle a difficult problem of time-of-flight operation at record accuracy. Preparations for this experiment are described in the accompany paper at this conference [3].

2 BYPASS LATTICE

The isochronicity of the bypass requires that the bypass be an achromat; and the dependence of the path lengths of electrons from energy, coordinate and angular deviations vanish. Theoretically, an achromat of the second order and higher can be made [4]. In practice, this has been proven to be impossible due to the tight space constraint in the planned experimental area. Therefore, in this design we aimed at finding a first-order achromat with weak second and higher order aberrations and large tolerance to errors.

As shown in Figure (1), the bypass lattice is mirror symmetric about the center. It contains one combined function magnet in the center, two approximately parallel faced dipole magnets, eight quadrupoles and six sextupoles.

After a careful selection of the first-order solution, aberrations above the second order become negligible and the second-order aberrations become weak. To minimize the remaining second-order aberrations, six sextupoles are placed in the bypass. The three independent sextupole strengths are fitted to minimize nine second-order time-of-flight matrix elements: T_{511}, T_{512}, T_{522}, T_{533}, T_{534}, T_{544}, T_{516}, T_{526}, T_{566} (in TRANSPORT notation). Each matrix element was considered to be small if the path length de-
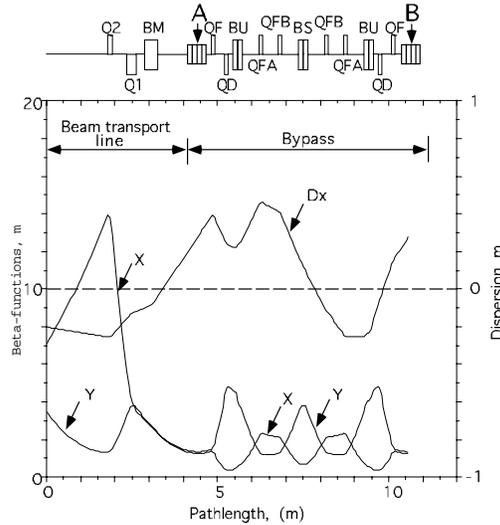
Figure 1: The beta-functions and the dispersion function of the bypass. Magnet locations, except sextupoles, are shown in the top.

viation associated with this coefficient at the end of fitting procedure fell below 0.1 μm. As a result, the ideal lattice, i.e. the lattice without errors, met all the constraints.

3 SIMULATION RESULTS

In order to have a detailed check of the isochronicity of the bypass lattice with errors, we performed a 'brute-force' particle tracking using code COSY INFINITY[5]. In all simulations we looked at the spread of the longitudinal coordinates of 10^4 electrons after their passage through the bypass. The electrons entered the lattice at the same time, but had distributions in energy, transverse coordinates and angles. We assumed that all beam distributions were Gaussian with the horizontal emittance $\epsilon_x = 1.1 \times 10^{-7}$ m·rad, the vertical emittance $\epsilon_y = 6 \times 10^{-8}$ m·rad and the relative energy spread $\sigma_{\Delta E/E} = 7 \times 10^{-4}$, as measured in [3].

At the beginning, we calculated the spread of path lengths for an ideal lattice without errors. The result of simulations with and without sextupoles correcting second order aberrations is shown in Figure (2). Without sextupoles, the spread of path lengths is not acceptable.

Then, we included static errors, i.e. errors due to manufacturing, assembly and calibration of the magnets, misalignment errors and tilt errors. Error specifications are given in Table I. (We assumed all errors having Gaussian
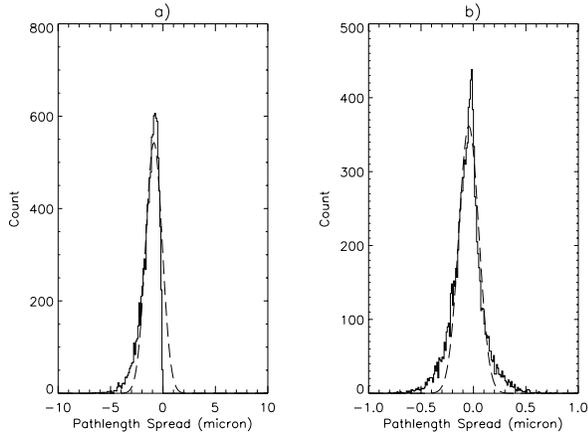
Figure 2: Histograms showing a spread of the pathlengths for the ideal lattice: a) without sextupole correction ($\sigma = 0.74\ \mu$m), b) with sextupole correction ($\sigma = 0.09\ \mu$m). Here and in subsequent similar pictures all sigmas are given for a fitted Gaussian distribution, which is shown by the dashed line. Note that the scale of the horizontal axis is ten times larger for the first histogram.

Table I: The specification of the errors.

	Static errors
Setting errors	$\sigma\left(\frac{\Delta B}{B}, \frac{\Delta G}{G}, \frac{\Delta S}{S}\right) = 1 \times 10^{-3}$
Tilt errors, [mrad]	$\sigma(\Delta\psi) = 0.2$
Misalignment errors in x, y, z [mm]	$0.15, 0.03, 1$
Multipole error [a]	
dipoles	$\sigma\left(\frac{b_3}{b_1}\right) = 1 \times 10^{-4}$ at $r = 3$cm
quadrupoles	$\sigma\left(\frac{b_3}{b_2}\right) = 5 \times 10^{-4}$ at $r = 5$cm
	Dynamic errors
Jitter in x, y	0.15 mm, 0.04 mm
Jitter in x', y'	0.10 mrad, 0.03 mrad
Energy jitter	0.5%
Power supply ripple	1×10^{-4}

[a] b_1, b_2 and b_3 are the dipole, quadrupole and sextupole components of the magnetic field.

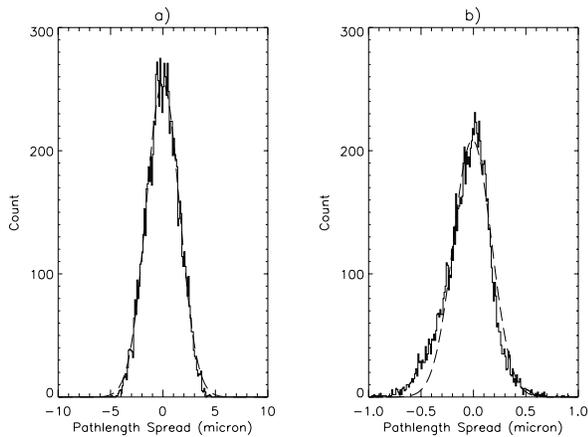Figure 3: Histograms showing a spread of the pathlengths due to the static errors: a) before correction ($\sigma = 1.57\mu$m), b) after correction ($\sigma = 0.181\mu$m). Note that the scale of the horizontal axis is ten times larger for the first histogram.
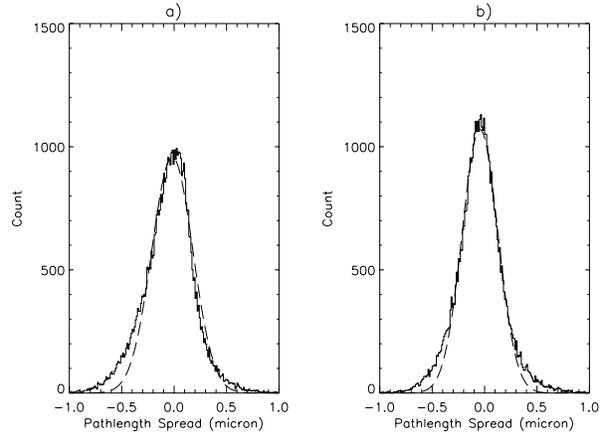

Figure 4: Histograms showing a combined effect of all static errors and all dynamic errors: a) first seed ($\sigma = 0.194\ \mu$m), b) second seed ($\sigma = 0.169\ \mu$m).

distribution truncated at $\pm 2.5\sigma$, where σ is the standard deviation of the distribution).

The static errors can be corrected to a certain extent using a beam-based correction technique. For example, as soon as static errors were added to the bypass lattice, the path length spread rose to about 1 μm (see the histogram in Figure 3a). This growth was mainly due to the setting errors leading to the linear distortions to the lattice. Tuning two families of quadrupoles, excited symmetrically (QF) and asymmetrically (QD), allowed us to reduce the spread to $\sim 0.2\ \mu$m (see, the histogram in Figure 3b).

There are also dynamic errors, i.e. errors that change each time the beam passes the bypass. They are smaller than static errors, but cannot be fixed with beam-based technique. Figure (4) shows the combined effect of all static and dynamic errors found in two seeds.

4 ANALYSIS

In this section we perform a quantitative analysis of the effect of time-of-flight errors. For this purpose we calculate the degree of coherence between the radiation fields of two undulators, which can be characterized by a dimensionless correlation function [6]:

$$\gamma\left(\tau\right) = \frac{\langle E_1(t)E_2^*(t+\tau)\rangle}{[\langle|E_1(t)|^2\rangle\langle|E_2(t)|^2\rangle]^{1/2}}$$
$$\simeq \exp\left\{-\frac{k^2\Delta\ell^2}{2}\right\}\exp\left\{-\frac{\Delta\omega^2\tau^2}{2}\right\}\exp\left\{i\omega_0\tau\right\}, \quad (1)$$

where $E_1\left(t\right)$ and $E_2\left(t\right)$ is the far field beam radiation in the first and second undulators, respectively, $\Delta\omega$ is the bandwidth of the radiation field, $k = \omega_o/c$ is the wave number, c is the speed of light and ω_0 is the central frequency of the radiation field. Averaging, denoted by the brackets $\langle...\rangle$, involves integration over a large time interval.

The second exponent in Eq.(1) shows that the coherence drops with the characteristic time scale $1/\Delta\omega$. The first exponent in Eq.(1) shows the effect of imperfections. It shows that the coherence drops with increasing particle longitudi-
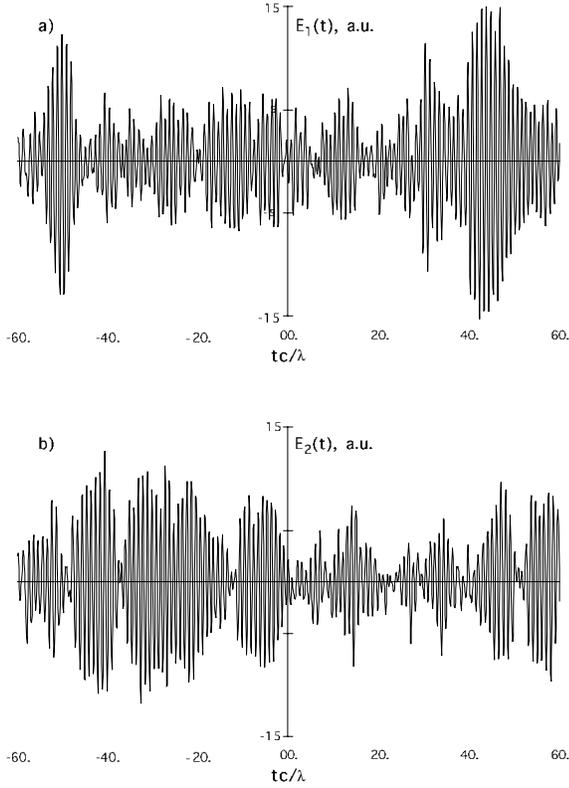
Figure 5: The field of beam radiation in the undulator with ten periods: a) the radiation field $E_1(t)$, b) the radiation field $E_2(t)$. Only a short pattern of the field near the center of the radiation pulse is shown.

nal mixing, $\Delta\ell$, during the beam passage between the two undulators.

We performed the simulation of the coherence of the fields of electron bunch radiation in the first and the second undulators with a 'brute-force' technique. In these simulations we assumed that the two undulators are identical and each undulator has ten undulator periods. The central wavelength of the radiation spectrum is $0.6\,\mu$m. First, we model the field $E_1(t)$ by taking a sum of the radiation fields of 10^4 electrons randomly distributed along the bunch with uniform average longitudinal density. An example of such a field is shown in Figure (5a). Then, we reproduce the actual mixing of the longitudinal coordinates of electrons within the bunch that occurs during the bunch passage through the bypass lattice and model the field $E_2(t)$. An example of this field is shown in Figure (5b). In this example we consider a case when all kind of errors are present (see histogram in Figure 4b).

Finally, we calculate the correlation function of two radiation fields and plotted it in Figure (6a). The maximum of the correlation function characterizes the degree of coherence between the radiation fields E_1 and E_2. It should be 1 if no mixing is present, but here it is dropped to 0.21. According to Eq.(1), this degree of coherence corresponds to $\Delta\ell = 0.171\,\mu$m (recalling that $\lambda = 0.6\,\mu$m), which is in
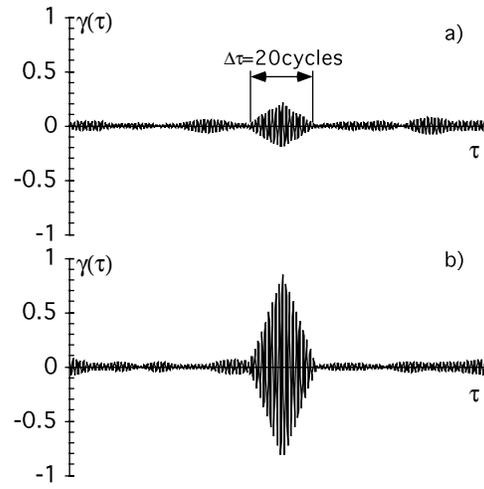

Figure 6: The correlation function of two radiation fields for a beam with the following parameters: a) $\epsilon_x = 1.1 \times 10^{-7}$ m·rad, $\epsilon_y = 6 \times 10^{-8}$ m·rad, $\sigma_{\Delta E/E} = 7 \times 10^{-4}$; b) $\epsilon_x = \epsilon_y = 10^{-8}$ m·rad and $\sigma_{\Delta E/E} = 3 \times 10^{-4}$.

good agreement with the spread of the pathlengths of 0.169 μm in Figure (4b). The degree of the coherence let us also conclude how machine imperfections and beam parameters effect damping time in Optical Stochastic Cooling. In the above example, we should expect approximately 5 times longer damping time, than in the ideal case.

Figure (6b) shows the correlation function calculated for the same lattice and with the same errors, but for $\epsilon_x = \epsilon_y = 10^{-8}$ m·rad and for $\sigma_{\Delta E/E} = 3 \times 10^{-4}$, i.e. for a beam parameters similar to the beams in the TEVATRON collider. The degree of coherence rose to 0.85. Thus, only 15% increase in the damping time is projected in this case.

5 CONCLUSION

We have designed a demonstration beam line to bypass the amplifier and to provide a necessary time delay in the method of Optical Stochastic Cooling. This involved designing a first-order achromat with corrections of the second-order geometrical and chromatic aberrations affecting the time-of-flight properties of the beam line. We have shown, by doing various simulations, that this beam line can meet design requirements with rather conservative tolerance to the errors.

6 REFERENCES

[1] A. Mikhalichenko and M. Zolotorev, Phys. Rev. Lett., v.71, 25, (1993)4146.

[2] M. Zolotorev and A. Zholents, Phys. Rev. E, v.50, N4, (1994)3087.

[3] A. Zholents et.al., this conf., Abstr. Log Number 5799.

[4] W. Wan and M. Berz, Phys. Rev. E, v.54, (1996)2870.

[5] M. Berz, Technical Report MSUCL-977, Michigan State University, (1995).

[6] S. Chattopadhyay et. al., Preprint LBNL-39788,(1997).